The Meteoritical Society

Meteoritics & Planetary Science 1–18 (2024)
doi: 10.1111/maps.14228

The reactivity of experimentally reduced lunar regolith simulants: Health implications for future crewed missions to the lunar surface

Donald A. HENDRIX[1,2]*, Tristan CATALANO[1], Hanna NEKVASIL[1], Timothy D. GLOTCH[1], Carey LEGETT IV[1,3], and Joel A. HUROWITZ[1]

[1]Department of Geosciences, Stony Brook University, Stony Brook, New York, USA
[2]National High Magnetic Field Laboratory, Florida State University, Tallahassee, Florida, USA
[3]Intelligence and Space Research, Los Alamos National Laboratory, Los Alamos, New Mexico, USA

***Correspondence**
Donald A. Hendrix, Department of Geosciences, Stony Brook University, Stony Brook, NY 11794-2100, USA.
Email: donh2015@gmail.com

(Received 08 March 2023; revision accepted 01 June 2024)

Abstract–Crewed missions to the Moon may resume as early as 2026 with NASA's Artemis III mission, and lunar dust exposure/inhalation is a potentially serious health hazard that requires detailed study. Current dust exposure limits are based on Apollo-era samples that spent decades in long-term storage on Earth; their diminished reactivity may lead to underestimation of potential harm that could be caused by lunar dust exposure. In particular, lunar dust contains nanophase metallic iron grains, produced by "space weathering"; the reactivity of this unique component of lunar dust is not well understood. Herein, we employ a chemical reduction technique that exposes lunar simulants to heat and hydrogen gas to produce metallic iron particles on grain surfaces. We assess the capacity of these reduced lunar simulants to generate hydroxyl radical (OH*) when immersed in deionized (DI) water, simulated lung fluid (SLF), and artificial lysosomal fluid (ALF). Lunar simulant reduction produces surface-adhered metallic iron "blebs" that resemble nanophase metallic iron particles found in lunar dust grains. Reduced samples generate ~5–100× greater concentrations of the oxidative OH* in DI water versus non-reduced simulants, which we attribute to metallic iron. SLF and ALF appear to reduce measured OH*. The increase in observed OH* generation for reduced simulants implies high oxidative damage upon exposure to lunar dust. Low levels of OH* measured in SLF and ALF imply potential damage to proteins or quenching of OH* generation, respectively. Reduction of lunar dust simulants provides a quick cost-effective approach to study dusty materials analogous to authentic lunar dust.

INTRODUCTION

Need for Lunar Dust Simulants for Human Health Studies

As early as 2026, the Artemis III mission will put humans back on the lunar surface for the first time in over half a century and preparations will begin for extended human stay. Of primary importance is ensuring the health of the astronauts in an environment hostile to life. Ubiquitous to the lunar surface environment is lunar regolith dust. From the Apollo era explorations, it became clear that lunar dust causes numerous problems, including interfering with lunar module controls, destroying vacuum seals in lunar sample vacuum chambers, and even tearing the outer layers of astronaut suits and boots. This dust also induced allergic responses in astronauts (Portree, 1997; Scheuring et al., 2008; Taylor, 2008). With plans for longer duration stays on the Moon's surface, dust exposure is likely to be a constant hazard to the astronauts, and the potential for detrimental effects on short- and long-term health of astronauts increases. It is

suspected that lunar dust, due to its unique chemistry, may lead to the development of health conditions, such as silicosis, chronic obstructive pulmonary disease (COPD), fibrosis, and other pulmonary hazards, as a result of exposure (Ehrlich et al., 2021; Fubini & Fenoglio, 2007; Fubini & Hubbard, 2003; Fubini et al., 2001; Hardy & Aust, 1995; Merchant et al., 1986; Sankila et al., 1990).

Lunar dust differs significantly from the dust commonly found on Earth. X rays and UV rays bombard the lunar surface which can lead to the formation of dangling bonds on the surface of particles and ionize atoms (Gaier, 2008). Early in the Apollo era, it was noted that irradiation of Apollo dust with high-energy protons affected the chemistry and altered reflectance spectra of dust (Hapke et al., 1970). It was noted at the Biological Effects of Lunar Dust Workshop in 2005 that lunar dust had a gunpowder-like smell to astronauts who removed their helmets inside the lunar module, which dissipated after a few hours (Allen, 2005; Gaier, 2008). This phenomenon may have been due to "activated" surface sites on lunar dust that were interacting with the olfactory cells of the crewmembers (Gaier, 2008). The dissipation of the smell may have been due to the passivation (i.e., "inactivation") of lunar dust particles upon exposure to the more humid cabin environment in the lunar module.

Irradiation of dust by high energy particles can result in the breakage of Fe-O linkages in a thin rind of crystals and reduction of the ferrous iron to metallic iron. Micrometeorite impacts (averaging fifty strikes per square meter per day) strike with very high kinetic energy at velocities greater than 10 km/sec, which produces sufficient thermal energy to melt and even vaporize lunar materials (Hörz et al., 1971). During this process, the metallic iron can be distributed throughout the melted material that rapidly cools down to form glassy "agglutinates" (Housley et al., 1973; Pieters et al., 2000). The proportion of agglutinates and metallic iron rise with decreasing grain size, which can lead to particles containing metallic iron getting trapped deep within the human respiratory system, including the alveolar regions (Glenn et al., 1986; Taylor & Meek, 2005). Agglutinates have an average 60-nm-thick rim of condensed amorphous silica (Keller & McKay, 1997). These silica glass rims are a cause for concern due to epidemiological evidence that silica glass increases both silicosis and lung cancer risks (Munn et al., 1990; Sankila et al., 1990; Wani & Niyogi, 1968). Exposure of dust-sized rock fragments on the lunar surface to solar particles, micrometeorite bombardment, and galactic cosmic rays can "activate" lunar dust, resulting in free radicals on the surfaces of lunar dust grains associated with "dangling bonds" (Liu & Taylor, 2011; Scully & Meyers, 2015). "Dangling bonds," lattice defects, strained lattices, surface radicals, metallic iron spheres, and agglutinates can remain unperturbed for extended periods of time in the high vacuum environment of the lunar surface. Apart from the very few Apollo astronauts, no humans have ever been exposed to such materials. Future lunar missions will last weeks to even months and there is high uncertainty regarding how such unique particulate matter may impact human health in the long term.

Reactivity studies are most relevant to lunar conditions if the dust simulant replicates the unique characteristics of lunar dust. There have been many attempts over the years to create lunar simulants that are realistic chemical, morphological, and structural proxies. Unfortunately, to date, there is no lunar simulant that is physically and chemically analogous to pristine lunar dust. The vacuum on the lunar surface (10^{-14}–10^{-12} torr), the low oxygen fugacity, the lack of water, and the constant micrometeorite impacts that are absent on Earth are all complicating factors in the production of lunar simulants that accurately mimic the chemical properties of lunar dust. This problem carries over into the practical assessment of a lunar dust particulate exposure limit (PEL). This limit has currently been set at 0.3 mg/m^3 by NASA (James et al., 2014). This limit is based on studies involving the exposure of mice to Apollo 14 lunar fines that spent decades in curation facilities on Earth. Long-term storage ameliorates the natural reactivity of particulate materials, resulting in the underestimation of the potential health hazards of lunar dust exposure (Loftus et al., 2010; Scully & Meyers, 2015).

This work attempts a more realistic assessment of lunar dust reactivity by using commercially available lunar dust simulants but conditioning them experimentally by "space weathering" to allow the formation of broken bonds, nanophase metallic iron on grain surfaces, and agglutinates. We do this via a simple reduction technique that uses both heat and hydrogen gas. Samples treated in this manner are referred to as "reduced" throughout this manuscript. Use of these samples to assess the oxidative nature and potential toxicological health effects of lunar dusts has the important additional benefit of removing the need to destroy precious Apollo samples.

Lunar Simulants Used in this Study

The Johnson Space Center-1 (JSC-1) simulant was developed in 1993 due to the need for a simulant with high glass content. This simulant was meant to replicate some of the properties observed in the Apollo 14 soils, particularly low-Ti mare soils. This parent material was quarried from a glass-rich basaltic tuff located on the south flank of Merriam Crater in the San Francisco volcano field near Flagstaff, AZ (McKay et al., 1994). JSC-1 mining operations were suspended and restarted again in the same location to produce JSC-1A. While JSC-1A accurately replicates particle size distribution

TABLE 1. Mineralogy and bulk chemical compositions of LMS-1,[a] LHS-1,[a] JSC-1A,[b] MLS-1,[b] and a typical Apollo[c] 11 and 16 soil/regolith breccia.

Oxide	JSC-1A	LMS-1	Apollo 11 (Mare soil)	LHS-1	Apollo 16 (Highland soil)
SiO_2	46.2	42.81	41.99	44.18	44.89
TiO_2	1.85	4.62	7.94	0.79	0.53
Al_2O_3	17.9	14.13	12.58	26.24	27.23
Cr_2O_3		0.21		0.02	
FeO	11.2	7.87	16.40	3.04	4.98
MnO	0.19	0.15		0.05	
MgO	6.87	18.89	7.93	11.22	6.00
CaO	9.43	5.94	11.74	11.62	14.56
Na_2O	3.33	4.92	0.47	2.30	0.47
K_2O	0.85	0.57		0.46	
P_2O_5	0.62	0.44			
SO_3		0.11		0.1	
Mineral abundances					
Glass-rich basalt	49.3	32.0	24.3	24.7	17.5
Pyroxene	0.01	32.8	44.9	0.3	8.5
Plagioclase	38.8	19.8	21.4	74.4	69.1
Olivine	9.0	11.1	2.1	0.2	3.9
Ilmenite	0.01	4.3	6.5	0.4	0.4
Quartz	0.2				
Amphibole	0				
Fe-Ti oxide	0.4				
Chrome spinel	1.1				
Sulfide	1				
Apatite	0.03				
Clay minerals	0.1				
Biotite	0				

Note: Lunar dust is the <20 μm diameter particles of lunar soil which can result in slight differences in composition (i.e., FeO content for Apollo 11 dust may be slightly lower versus Apollo 11 soil and vice versa for Apollo 16 lunar dusts and soil).
[a]Data from the Center for Lunar & Asteroid Surface Science (CLASS) Exolith Lab.
[b]Data from Hill et al. (2007).
[c]Data from Table A8.1 in *The Lunar Sourcebook*.

(PSD) and a few other physical properties, such as abrasiveness, its mineralogy, and chemistry, do not accurately replicate significant portions of the lunar regolith (Hill et al., 2007). However, other workers have used JSC-1A for assessing the ability to generate OH* in deionized (DI) water; we, therefore, use it in our studies to enable comparison to their studies (Hendrix et al., 2019; Kaur et al., 2016; Wallace et al., 2010).

The Center for Lunar and Asteroid Surface Science (CLASS) Exolith lab at the University of Central Florida has produced two lunar simulants that we use here, lunar mare simulant-1 (LMS-1) and lunar highland simulant-1 (LHS-1). While both simulants mimic average modal mineral proportions of the lunar highlands and mare well, the chemistries of these simulants still do not perfectly reflect lunar chemistries. Both contain higher sodium and potassium contents and lower levels of Fe, Mg, and Ca than typical lunar regolith, which highlights some of the caveats of using regolith simulants that are composed of terrestrial minerals and glass. Finally, a key drawback to all simulants is the lack of components that mimic Fe particles and agglutinates. For reference, Table 1 shows the mineralogy and constituent oxide concentrations for LMS-1, LHS-1, JSC-1A, and a typical Apollo 11 (mare) and 16 (highland) soil.

OH* Generation Studies

OH* generation measurements of various dusts that pose potential inhalation health risks have been performed as a proxy for direct assessment of potential adverse inhalation health effects due to the highly toxic nature of OH* and its ability to induce DNA damage (Angelé-Martínez et al., 2014; Dizdaroglu et al., 1991; Pryor, 1988; Von Sonntag, 1991). Radicals can lead to oxidative stress in the lungs, resulting in the apoptosis of epithelial and endothelial cells, which may then induce inflammatory responses that prevent the removal of

inhaled particulate matter (Xu et al., 2020). Various studies have assessed both the OH* and hydrogen peroxide generation capacity of lunar analog dusts ground by hand (Hendrix et al., 2019; Hurowitz et al., 2007; Kaur et al., 2016; Turci et al., 2015; Wallace et al., 2009, 2010). Hand-grinding is meant to replicate the mechanical alteration experienced by lunar dust during micrometeorite bombardment, which results in dangling bonds and other surficial defect sites (Loftus et al., 2010; Wallace et al., 2009). The hand-grinding process exposes surficial ferrous iron atoms, and these studies have proposed that this permits the Fenton reaction to generate OH* in solution through the interaction of H_2O_2 and surface-bound Fe-atoms. Equation (1) shows the Fenton reaction (Fenton, 1894).

$$\equiv Fe^{2+} + H_2O_2 \rightarrow \equiv Fe^{3+} + OH^* + OH^- \quad (1)$$

As a representative example that shows the role that iron plays in determining particulate reactivity, Figure S1 (supplement), from Hendrix et al. (2019) (their Figure 6), shows surface area normalized OH* generation of various mineral phases, as well as JSC-1A (Hendrix et al., 2019). Olivine is the most reactive mineral of those investigated; the reactivity for every other mineral begins to decline to ~1μmole OH*/m^2, generally tracking the decrease in bulk iron concentration between minerals. The JSC-1A simulant, which is a mixture of Fe-rich and Fe-poor phases, generates intermediate OH* concentrations.

Wallace and co-workers studied the reactivity of eight Apollo dust samples (Wallace et al., 2009, 2010). To our knowledge, these are the only studies that experimentally assessed the ability of Apollo samples to generate OH* in solution. They made the following key observations: mare samples generate more OH* than highland samples, consistent with the aforementioned conclusion that iron plays an important role in particulate reactivity. JSC-1A, the mare basalt simulant, generated less OH* than the least reactive lunar highland sample, consistent with the notion that this regolith simulant does not adequately represent the reactivity of lunar regolith. Finally, they determined that increased regolith "maturity," which is another way to express the degree to which a regolith sample has been space weathered, results in an increased ability to generate OH* (Wallace et al., 2010). The evidence points to iron, and specifically metallic iron, as playing an important role in the mechanisms that generate OH* in solution (Wallace et al., 2010). Wallace et al. (2010) suggested that grinding mature lunar regolith in air and exposing them to solution would oxidize metallic iron to ferrous iron which would then allow for large quantities of OH* to be generated via Fenton chemistry, when compared to that produced by terrestrial material-based simulants such as JSC-1A. However, the short timescales of typical reactivity experiments may not result in significant Fe-oxidation, and we suggest that is also possible that metallic iron plays a direct role in Fenton-style chemistry, with metallic iron acting as an electron donor that generates OH* by reduction of H_2O_2.

Assessment of OH* Generation in Biologically Relevant Fluids

This study uses both simulated lung fluid (SLF) as well as artificial lysosomal fluid (ALF) and assesses the potential of JSC-1A, LMS-1, and LHS-1 in their reduced and non-reduced forms to generate OH* in biologically relevant fluids. These fluids have been used in a multitude of studies assessing the bioaccessibility of road dusts, airborne particulate matter (APM), and other respirable compounds (Colombo et al., 2008; Kastury et al., 2018; Midander et al., 2007; Pelfrêne et al., 2017; Stopford et al., 2003; Wiseman, 2015). Human extracellular and lysosomal fluids contain a complex array of surfactants, complex proteins, and enzymes; the simulated biological fluids in our study contain citrate, amino acids, and dipalmitoylphosphatidylcholine (DPPC) which are meant to replicate the complex organics and proteins present in lysosomal and extracellular fluids (Brain, 1992; Pelfrêne et al., 2017). DPPC is a phospholipid and is the most abundant surfactant secreted by type II alveolar cells (Morton, 1989). ALF replicates the fluid inside alveolar macrophages. The action of alveolar macrophages, cells responsible for maintaining a sterile respiratory environment by removing foreign particulate matter including dust, viruses, and other pathogens, and translocation of particles into the interstitium for subsequent drainage to the lymph nodes are two mechanisms by which particulate matter is cleared from the lungs (Brain, 1992). Exposure to toxic particulate matter may hinder these processes (Bos et al., 2019; Xu et al., 2020). Studies that have assessed the bioaccessibility of particulate matter, as well as APM have found that the bioaccessibility of metals in ALF is significantly higher than in SLF (Kastury et al., 2018; Meza-Figueroa et al., 2020; Pelfrêne et al., 2017; Weggeberg et al., 2019). This was mostly attributed to the lower pH of ALF versus SLF. While our study is focused on OH* generation, the fact that more metals are leached into solution in ALF highlights the potential risks of lunar dust exposure beyond just the release of free radicals. Release of metals such as Fe, Cu, Ni, Co, and Cr has been linked to inflammatory responses in type II alveolar cells of mice (He et al., 2017). Trace elements, such as K, Rb, Cs, and Ce, are present in lunar regolith in concentrations as high as nearly 10,000 μg/g, which may have deleterious health consequences if they undergo

geochemical speciation when in contact with biological fluid (Heiken et al., 1991).

Reduced Lunar Simulants for Human Health Studies

Previous works have used lunar simulants and Apollo samples to understand the potential environmental health hazards associated with lunar dust exposure (Brady et al., 2020; Caston et al., 2018; Heiken et al., 1991; Hendrix et al., 2019; Hill et al., 2007; Hurowitz et al., 2007; Kaur et al., 2016; Li et al., 2019; Linnarsson et al., 2012; Taylor et al., 2016; Wallace et al., 2009, 2010). Some of these lunar simulants, such as JSC-1A do not reflect the average mineralogical compositions of the lunar mare or highlands, and the reactive properties of Apollo samples may be compromised by long-term storage on Earth (Hill et al., 2007; Lam et al., 2013; Loftus et al., 2010; Scully & Meyers, 2015). The elemental concentrations of Fe and Ca are generally higher, while concentrations of Na, K, and Mg are lower in lunar samples versus terrestrial materials. Our work centers around assessing the effect of metallic iron, a non-terrestrial component of lunar dust, which is suspected to have a disproportionate effect on Fenton chemistry relative to any ferrous iron present in our samples (Liu et al., 2007; Wallace et al., 2010). A key drawback to any currently available lunar simulant is the absence of the glassy silica rims and submicroscopic-iron (SMFe). How such particles can affect human health is poorly understood. We use a reduction technique involving heat and hydrogen gas, similar to the technique used in Allen et al. (1994), to generate surface adhered metallic iron particles in our three lunar simulant samples, JSC-1A, LMS-1, and LHS-1 (Allen et al., 1994). Our reduction technique allows for an assessment of the environmental health risks posed by exposure to space weathered lunar dust during future crewed missions to the lunar surface without reliance on precious Apollo dust samples or lunar simulants that may inaccurately replicate lunar dust reactivity in their as-received state. The chemical reduction technique described here can be used to produce experimentally space weathered lunar simulants "on-demand" in large quantities (~grams) for other assays such as cell toxicity and animal studies. A just-published study by Chang et al. (2024) used the lunar dust simulant samples described in this work and found significant increases in cytotoxicity for the reduced dust simulants. Their results are further discussed at the end of this manuscript.

This work addresses a few of NASA's Strategic Knowledge Gaps, particularly those listed under Theme 2 —*Understand the Lunar Environment and Its Effects on Human Life* (Shearer et al., 2016). We also expand on some knowledge gaps outlined in the report following the Impact of Lunar Dust on Human Exploration Workshop, including estimating the potential long-term effects of lunar dust exposure to humans as well as understand how lunar nanoparticles may react with biologically relevant fluids (Brady et al., 2020). Here, we present the first experimental observations of OH* generation of the lunar simulants, LMS-1 and LHS-1, and the OH* generation of experimentally reduced forms of all three lunar simulants (JSC-1A, LMS-1, and LHS-1) in widespread use.

METHODS

Milling and Reduction of Lunar Simulants

As-received lunar simulants were sieved using a 63-μm mesh sieve and 10 g of sieved simulant were then milled in a pre-cleaned Retsch PM 100 ball mill grinder for 2 h at 350 rpm under benchtop conditions. Seven 20-mm-diameter agate balls were used in a 125-mL agate mortar. All samples were ground for four 30-min intervals with approximately 5 min of rest in between each interval to prevent overheating of the sample. The temperature of the simulants was not monitored during grinding. Milled samples were stored in a desiccator before use in analysis or experiments. Milled samples allocated for OH* measurement were left exposed to atmosphere on the benchtop for two weeks to passivate any surface defect sites or surface radicals formed due to the milling process (Hendrix et al., 2019; Wallace et al., 2009).

Reduction experiments were performed just before the sample was to be analyzed to minimize the risk of post-reduction oxidation of the samples. To reduce the simulants, three grams of milled material were loaded into a silica boat, which was placed in the middle of a horizontal silica glass tube. The tube was then sealed at either end by one-hole rubber stoppers that allow gas to flow through the tube from the gas tank to a flask of vacuum pump oil. The gas bubbled through vacuum pump oil at the vent in order to prevent ingress of air through the vent and as a qualitative check of the hydrogen flow. The rubber stoppers were far from the heat source so there was no risk of the rubber stoppers melting. The tube was flushed with pure H_2 gas for 10 min before heating. The tube assembly was then placed in a furnace with a monitoring Type K thermocouple and the furnace was turned on. Furnace voltage was controlled by a Variac voltage regulator, and the temperature was determined by the monitoring thermocouple. Once the furnace reached the target temperature of 950 °C, the reaction was allowed to continue for 15 min at the target temperature. After the 15-min roasting process, the furnace was turned off and the silica glass tube immediately removed and cooled. Cooling was done by first blowing pressurized air on the silica tube until the sample was no longer glowing (roughly 650 °C), then by applying wet towels to the tube. Once cool, the flow of H_2

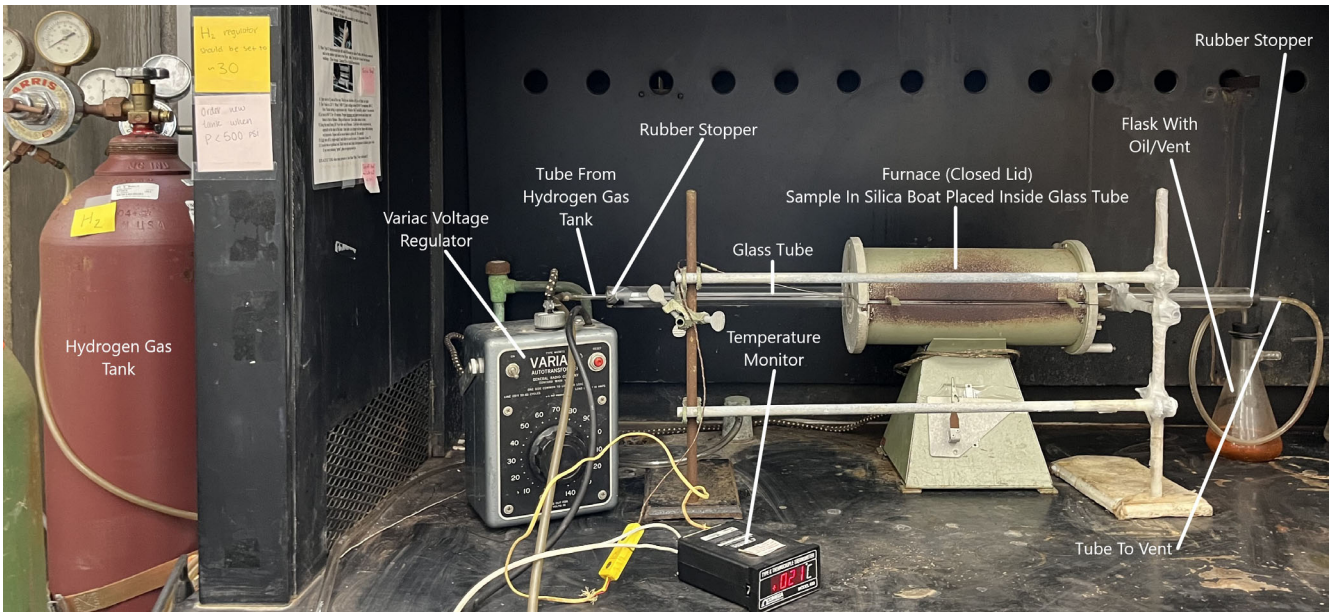

FIGURE 1. Labeled image showing the setup of the furnace used for the hydrogen reduction experiments of the lunar dust simulant samples.

was stopped, the sample was removed from the silica tube and quickly placed in a labeled vial and stored in a Thermo Scientific Lab-Line vacuum desiccator at approximately ~25 mmHg to inhibit reaction with atmospheric oxygen. Samples were removed from the desiccator as needed for OH* analysis, briefly exposing samples to air. Figure 1 shows the setup of the reduction technique.

Biologically Relevant Fluids

SLF and ALF were produced using the same recipe as Pelfrêne et al. (2017). Table 2 lists the concentrations (g/L) used in our experiments for all reagents used to formulate both SLF and ALF. Components of SLF and ALF were dissolved in DI water that had been kept in the dark for more than 30 days to minimize any potential OH* generation due to photooxidative effects. SLF and ALF were stored at 3–4 °C for up to 14 days and made fresh as needed. Table S1 lists the component names, chemical formulas, vendors, and catalog numbers of the reagents.

OH* Generation Measurements

Aliquots of 200 mg of each lunar dust simulant were ground for 5 min by hand in an agate mortar and pestle. Agate ensures minimal contamination of the samples (Hickson & Juras, 1986). Ground samples were added to Al foil-wrapped centrifuge tubes containing 0.5 mL

TABLE 2. Composition of ALF and SLF used in this study.

Composition (g/L)	Formula	SLF	ALF
Citric acid			20.0[a]
Sodium chloride	NaCl	6.779	3.21
Sodium phosphate dibasic	Na_2HPO_4		0.071
Sodium bicarbonate	$NaHCO_3$	2.268	
Trisodium citrate dihydrate	$C_6H_5Na_3O_7{\cdot}2H_2O$	0.055	0.077
Ammonium chloride	NH_4Cl	0.535	
Glycine	$C_2H_5NO_2$	0.375[b]	0.059[a]
Sodium dihydrogen phosphate	NaH_2PO_4	1.872	
L-cysteine	$C_3H_7NO_2S$	0.121[b]	
Sodium hydroxide	NaOH		6.0[a]
Calcium chloride dihydrate	$CaCl_2{\cdot}2H_2O$	0.026	0.128
Sodium sulfate	Na_2SO_4		0.039
Magnesium chloride hexahydrate	$MgCl_2{\cdot}6H_2O$		0.05
Disodium tartrate	$C_4H_4Na_2O_6$		0.09[a]
Sodium lactate	$NaC_3H_5O_3$		0.085[a]
Sodium pyruvate	$C_3H_3NaO_3$		0.172[a]
DPPC	$C_{40}H_{80}NO_8P$	0.1[a]	

Abbreviation: DPPC, dipalmitoylphosphatidylcholine.
[a]OH* generation of San Carlos olivine powder was measured in noted individual solutions.
[b]OH* generation of San Carlos olivine was measured in a solution of both noted components mixed into one.

88.4 mM 5,5-dimethyl-1-pyrroline-N-oxide (DMPO) (Santa Cruz Biotechnology) plus 0.5 mL of DI water, SLF, or ALF at a particle loading of 100 m^2/L. The resulting mineral slurry was incubated on a Barnstead 400110 end-over-end tube rotator for 15 min. The slurry was filtered into a plastic vial using a 13 mm Millex-GN 0.02 μm and a BD 3-mL Luer-Lok™ Tip syringe filter. Three 50-μL aliquots of filtrate were then pipetted into three separate 50-μL Hirschmann ISO 7550 glass capillary tubes. Each capillary tube was sequentially placed in the sample chamber of a Magnettech MS400 Mini-Scope X-band electron paramagnetic resonance (EPR) spectrometer to measure generated OH*. The OH* concentrations derived from each aliquot were averaged to yield a triplicate measurement. The calibration standard 4-hydroxy-2,2,6,6-tetramethylpiperidin (TEMPOL) (Santa Cruz Biotechnology) was used to generate a calibration curve for use in the calculation of the concentration of OH* of each slurry; methods are explained in detail in Hendrix et al. (2019) (Eaton et al., 2010). Four TEMPOL concentrations, 0.5, 1.0, 2.0, and 3.0 μM were used to generate the calibration curve. EPR parameters are listed in Table S2.

In addition to the simulant measurements, a set of OH* measurements using San Carlos olivine, identical to that used in Hendrix et al. (2019), was analyzed for OH* generation in SLF, ALF, DI water, and in various individual components of both biological fluids described in Table 2 (Hendrix et al., 2019). All spin-trap compound, calibration, incubation, filtration, and EPR measurements were performed as described above. San Carlos olivine was chosen due to its known capability to generate measurable OH* in solution, and the purpose of these additional measurements was to understand the influence of the individual components of SLF and ALF, at various concentrations, on OH* generation. These measurements used a particle loading of 400 m^2/L to ensure a high signal-to-noise ratio during EPR measurements. Approximately 136 mg of olivine were ground in an agate mortar and pestle for 5 min prior to OH* generation analysis. The same particle loading was used to measure OH* generation in a total of 8 separate solutions of both glycine and cysteine at concentrations of 0.0, 0.05, 0.10, 0.25, and 0.50 g/L.

Solid Phase Characterization

Grain sizes were measured using a Malvern Instruments Mastersizer 2000 which uses Mie scattering intensity to determine particle size distribution of powders. A Quantachrome Instruments Nova 2200e analyzer was used to determine the surface area of each sample using the Brunauer–Emmet–Teller (BET) theory for N_2 gas adsorption. An aluminum oxide reference standard (Anton Paar) with surface area 14.26 m^2/g was run in parallel with each sample. Scanning electron microscopy (SEM) images were obtained using a LEO-1550 FEG SEM equipped with an energy dispersive X-ray (EDX) spectrometer. All samples were twice coated with a 2-nm gold layer using an Edwards 150B sputter coater at a 30° angle prior to SEM/EDX analysis. Reflectance spectra in the visible near-infrared (VNIR) were collected using an ASD FieldSpec 3 Max spectrometer with a bidirectional (30° incidence and 0° emergence angles) configuration. Samples were placed into the sample holder (~2.2 mm thickness) which was then gently tapped to make a flat surface. Spectralon was used as a reflectance reference. Each sample was rotated 90° for each measurement for a total of four measurements which were then averaged into one final spectrum. Final spectra were corrected to absolute reflectance to remove the spectral features attributed to the Spectralon standard. A Rigaku MiniFlex 600 X-ray diffractometer (XRD) was used to observe changes in metallic iron presence between non-reduced and reduced lunar simulants. Table S3 lists the reagents used in this study outside of the preparation of SLF and ALF.

RESULTS

Experimental Reduction of Lunar Simulants—Solid Phase Characterization

Clear evidence for the generation of metallic iron by reduction is shown by the comparison of PXRD (powder X-ray diffraction) patterns of reduced and non-reduced versions of each simulant in Figure 2a–c. The three primary α-Fe peaks lie at $2\theta = 45°$, 65°, and 82°. The PXRD pattern of reduced JSC-1A exhibits strong alpha iron peaks at 2θ of 45° and 82° and a weak peak at 2θ of 65°. The PXRD pattern of reduced LMS-1 exhibits a strong α-iron peak at 2θ of 45° and two weak peaks at 2θ of 65° and 82°. The PXRD pattern of reduced LHS-1 exhibits two weak α-iron peaks at 2θ of 45° and 82°; these weak peaks are consistent with the Fe-poor nature of composition LHS-1. None of the non-reduced simulants exhibit peaks for α-Fe.

Reflectance spectra (Figure 3a–c) indicate loss of spectral features, reduced overall albedo, and spectral reddening (an increasing spectral slope from short to long wavelengths) for all lunar dust simulants compared to the non-reduced simulants. Spectral reddening has been observed for lunar dust samples and is primarily attributed to the presence of SMFe spherules that result from space weathering (Hapke, 2001; Thompson et al., 2016).

Figure 4a–f shows SEM images of each simulant in its reduced and non-reduced forms. Reduced JSC-1A, LMS-1, and LHS-1 were all seen to contain surface adhered

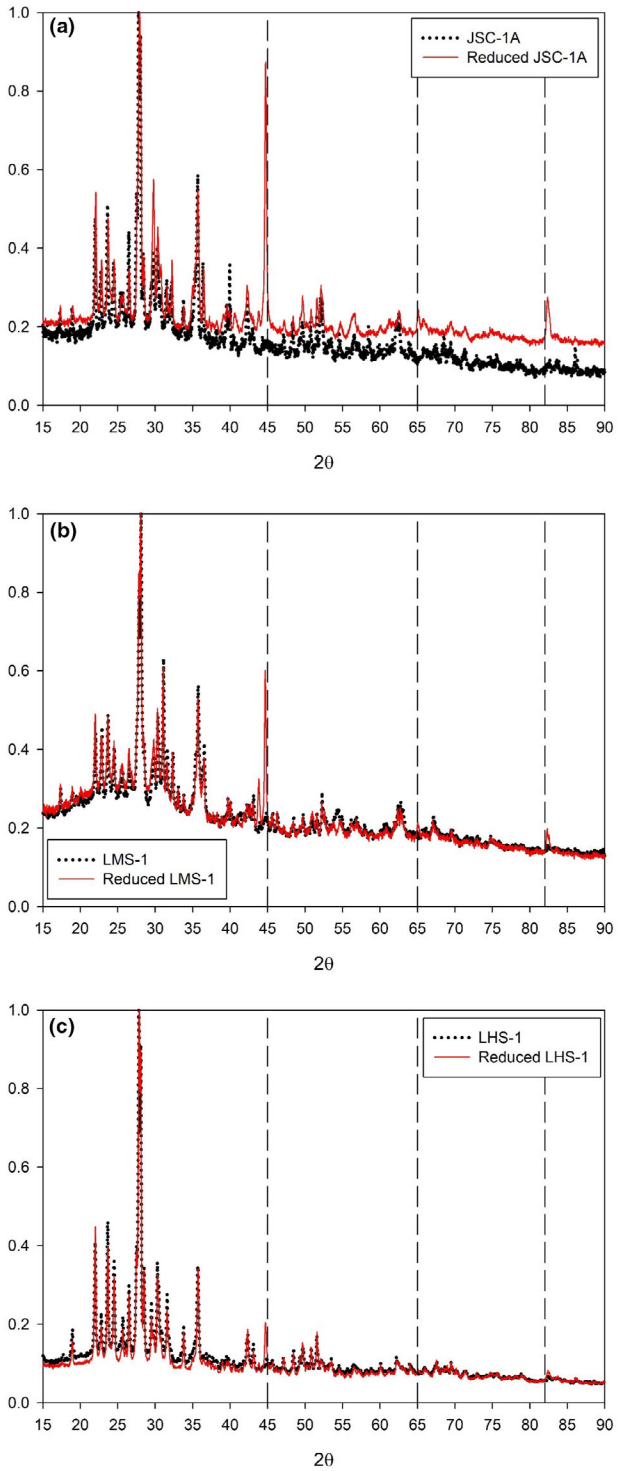

FIGURE 2. XRD patterns for reduced and non-reduced (a) JSC-1A, (b) LMS-1, and (c) LHS-1. Dashed vertical lines show peak positions for α-Fe ($2\theta = 45°$, 65°, and 82°).

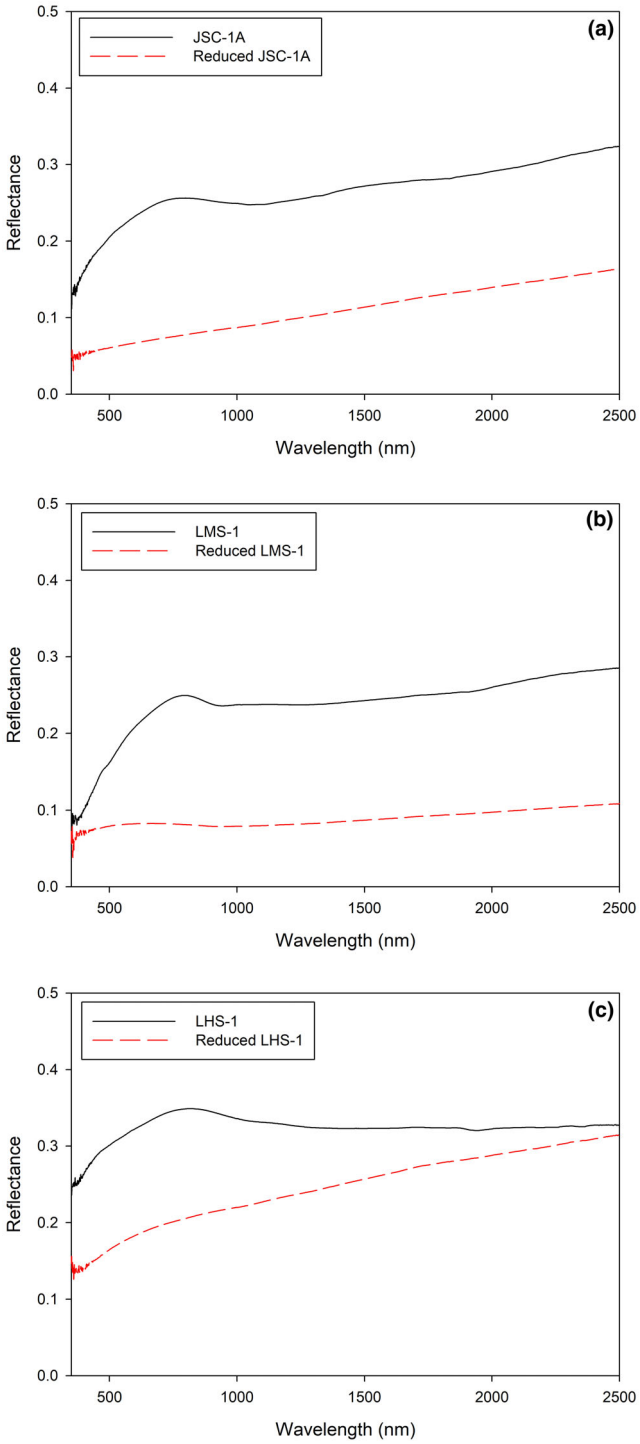

FIGURE 3. Spectral reflectance (0.5–2.5 μm) of reduced and non-reduced (a) JSC-1A, (b) LMS-1, and (c) LHS-1.

spherules that are bright in SEM images (Figure 4a,c,e), indicating that they contain high concentrations of high-Z elements relative to their surroundings. The spherical blebs are generally ~100 nm in diameter and are not present on any of the images of non-reduced simulants (Figure 4b,d,f). These blebs are similar in appearance to the metallic iron blebs observed by Allen et al. (1994) in their

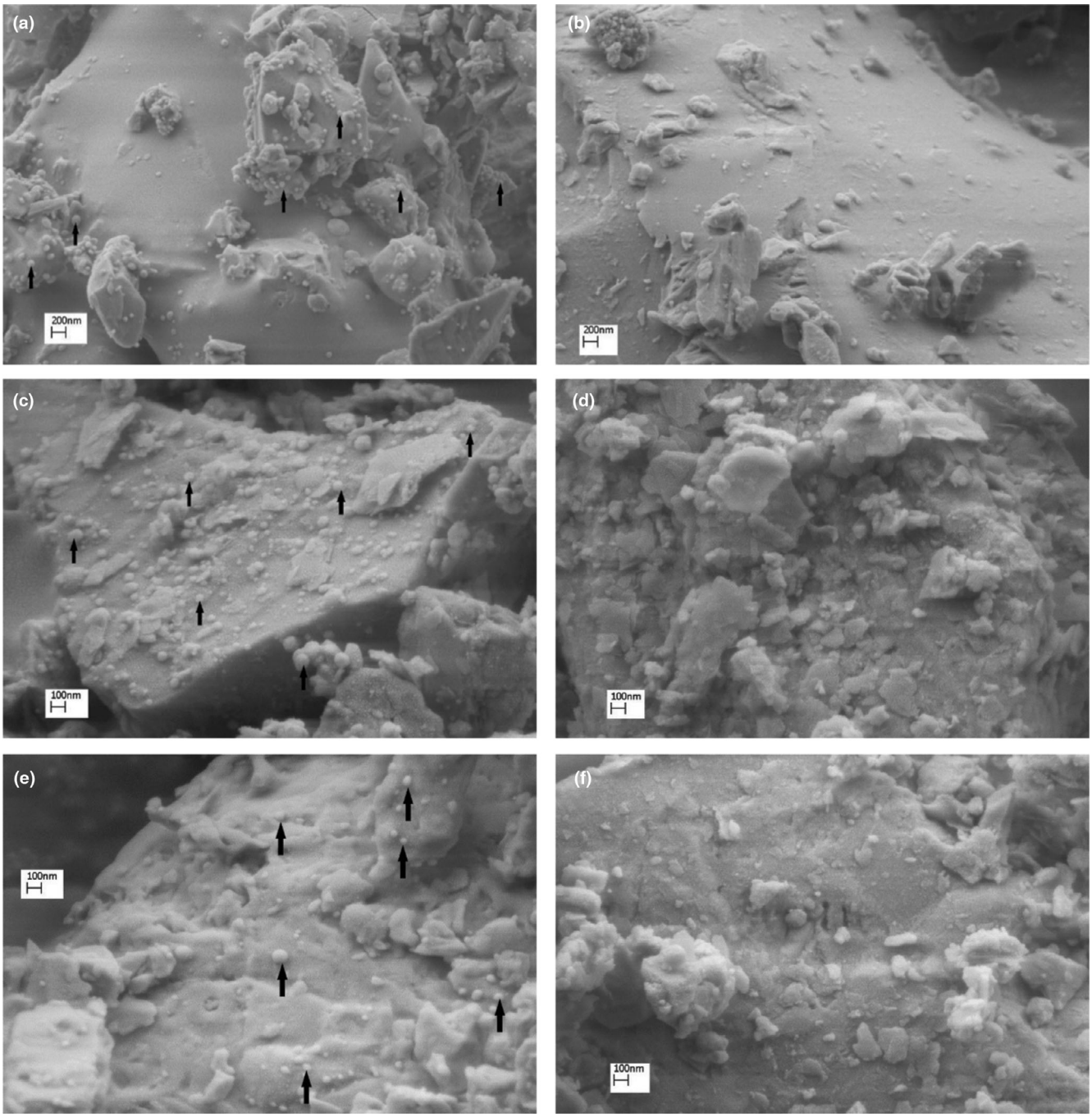

FIGURE 4. SEM images of (a) reduced JSC-1A, (b) non-reduced JSC-1A, (c) reduced LMS-1, (d) non-reduced LMS-1, (e) reduced LHS-1, and (f) non-reduced LHS-1. Black arrows in (a), (c), and (e) denote ~100 nm diameter, approximately spherical blebs that decorate the surface of the simulants; these blebs are not observed in images of non-reduced simulants.

experimentally reduced simulants (Allen et al., 1994). Figure 5a–f shows SEM images and EDS spectra collected from reduced simulants. Owing to the extremely small size of the iron blebs, the EDS spectra are not only derived solely from the blebs but also include some of the material around the blebs. Nevertheless, the regions that include the small bright blebs appear to be iron rich compared to their surroundings, consistent with the conclusion that these blebs are Fe.

Allen et al. (1994) observed that ilmenite ($FeTiO_3$) was the mineral that was most susceptible to reduction and produced the largest proportion of surficial metallic iron, followed by olivine and pyroxene (Allen et al., 1994). Our lunar simulants contain these three minerals

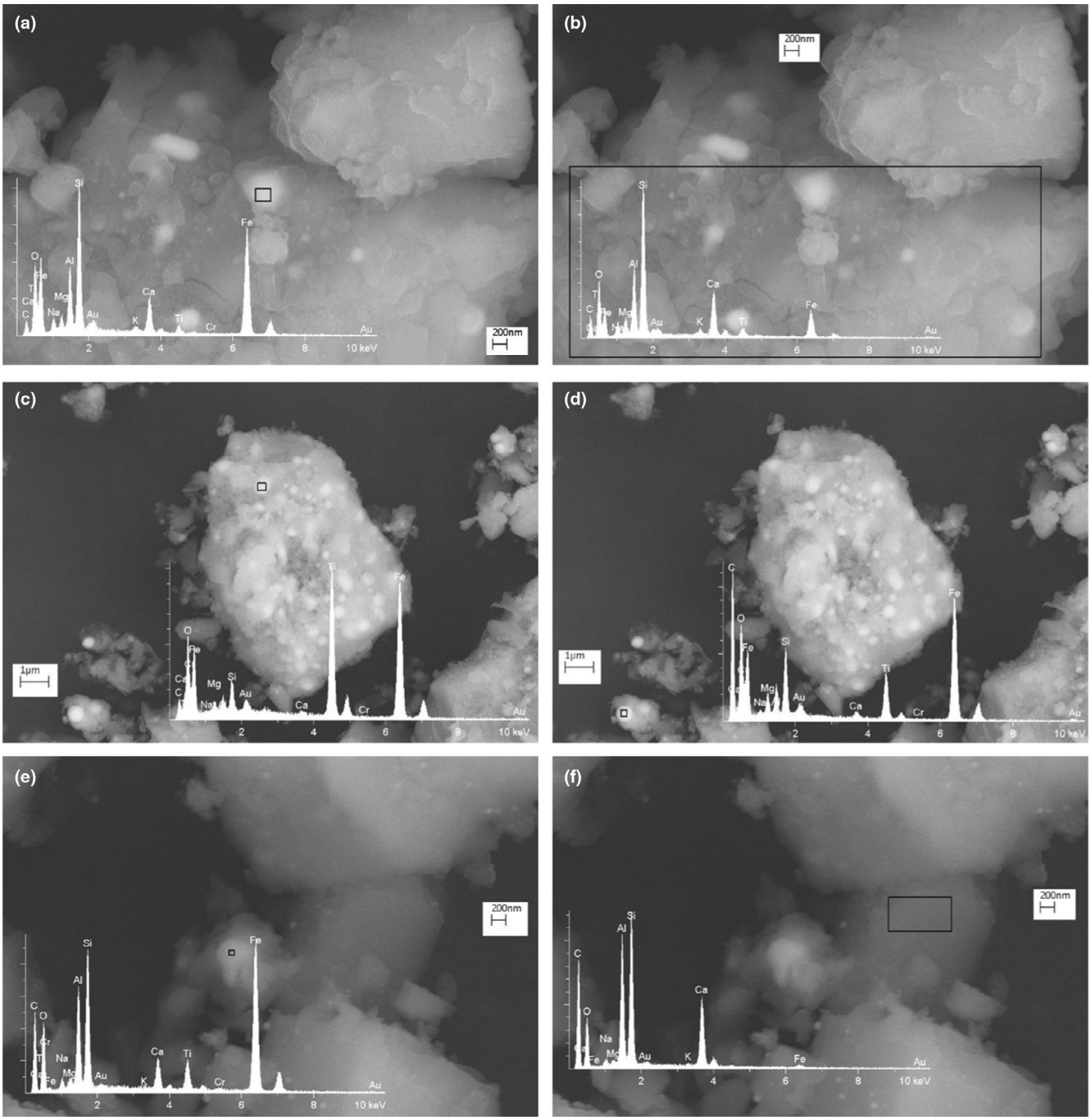

FIGURE 5. SEM images and inset EDS spectra of areas analyzed (indicated by black boxes). (a) EDS spectrum of small bleb on reduced JSC-1A, (b) EDS spectrum of large area of reduced JSC-1A from the same imaging location. Note differences in the Fe-peak height between (a) and (b). (c) EDS spectra of iron bleb on reduced LMS-1 and (d) of the entire image area for LMS-1. Note high abundance of Ti in (c). (e) EDS spectrum of small bleb on reduced LHS-1, (f) EDS spectrum of mineral grain without Fe-bleb from the same imaging location.

and appear to exhibit similar behavior. For example, bright blebs in LMS-1 also appear to be associated with large X-ray fluorescence peaks associated with Ti (Figure 5c) or Si and Mg (Figure 5d), consistent with derivation from an Fe-Ti oxide and olivine, respectively. In other cases, a direct link to a precursor Fe-bearing mineral phase is less clear. For instance, in Figure 5a, the bright bleb not only has a large Fe peak but is also associated with Na, Si, Al, and Ca peaks, which are likely derived from plagioclase feldspar. Plagioclase feldspar is

nominally an Fe-free mineral, so the apparent association between bright, Fe-rich blebs and plagioclase is most likely caused by reduction of Fe oxide or ilmenite inclusions in the plagioclase. In an SEM image of LHS-1, a bright region appears to be associated with elevated Ti (Figure 5e), consistent with ilmenite in plagioclase.

Heat treatment/reduction had a minimal impact on median grain size but caused a significant decrease in surface area (Table 4). This may be due to a sintering effect that results from our reduction method, which was also apparent in the physical properties of the simulants after hydrogen reduction; the simulants appeared to clump together and required some mechanical disaggregation to return to its original powder state, similar to the cohesive properties of lunar agglutinates. Disaggregation involved manually breaking up the clumped material with a steel sample spoon. Since the sample size required by some analytical and experimental techniques was very small in comparison to the amount produced, it was broken up to a roughly powdery state leaving few or no clumps larger than roughly 1–2 mm. The most significant decrease in the surface area post reduction was of LMS-1 (~66%). Raw data for surface areas of lunar simulants and standards can be found in Tables S5 and S6. We also observed visible darkening of each lunar dust simulant after reduction/heat treatment, consistent with the VNIR spectra shown in Figure 3. At visible wavelengths, nanophase metallic Fe particles are strong absorbers, leading to an overall darkening of mature (space weathered) lunar regolith compared to immature regolith of the same composition. Tables S4–S6 show the raw data for the lunar simulant grain sizes, lunar simulant surface areas, and surface area standards. Figure S2 (supplement) shows the graphical PSD for each reduced and non-reduced lunar simulant.

OH* Generation of Lunar Simulants

Averages and standard deviations of three measurements of OH* generated in solution for all lunar simulant samples are shown in Table 3. Figure 6a–c compare the generation in solution of OH* for both reduced and non-reduced JSC-1A, LHS-1, and LMS-1 in DI water, SLF, and ALF. There is a significant increase in reactivity in the reduced samples. Importantly, the amount of FeO in the starting materials does not seem to affect reactivity.

Significantly less OH* was measured in solution for all reduced lunar simulants in both SLF and ALF (Figure 6b,c). In SLF, there was no statistical difference in OH* generation between reduced and non-reduced LHS-1, while the measured OH* concentration for reduced LMS-1 and JSC-1A was slightly higher than their non-reduced counterparts. In ALF there was no difference in OH* production in reduced or non-reduced samples, and in fact, all measured OH* concentrations in ALF are considered non-detections within the reproducibility of our measurements.

Which components of SLF and ALF were the primary players in causing the small amount of OH* production by the simulants was explored using the mineral olivine because the OH* generation of this mineral has been studied previously (Hendrix et al., 2019, 2021). Samples of San Carlos olivine were exposed to SLF, ALF, and various individual components of those fluids. In the case of SLF, we focused on measuring olivine reactivity in pure SLF, in an amino acid mixture of 0.375 g/L glycine +0.121 g/L cysteine in SLF (SLF AA in Figure 7) and in the DPPC surfactant in SLF, ignoring the non-redox active inorganic components also present in SLF. As shown in Figure 7a, SLF caused a significant decrease in OH* production by olivine relative to DI water, indicating that the behavior of olivine in SLF is similar to that seen for lunar regolith simulants. Figure 7a also shows that the DPPC surfactant is not responsible for the decrease in OH* production in SLF. In contrast, however, the mixture of the amino acids cysteine and glycine in SLF seems to substantially reduce the OH* generating capacity of olivine, suggesting that these amino acids may be responsible for the low measured concentrations of OH* in SLF.

Figure 7b shows OH* production with varying amounts of cysteine and glycine, from 0 g/L (DI water) to 0.5 g/L, which includes the concentration range of these amino acids in SLF and ALF. As shown, glycine does not reduce OH* production across the full concentration

TABLE 3. Measured OH* generation in solution for lunar simulants.

	JSC-1A	LHS-1	LMS-1	JSC-1A (R)	LHS-1 (R)	LMS-1 (R)
DI water	0.105 ± 0.038	0.006 ± 0.022	0.031 ± 0.019	0.563 ± 0.249	0.658 ± 0.033	0.736 ± 0.025
SLF	0.030 ± 0.018	0.003 ± 0.018	0.017 ± 0.016	0.084 ± 0.015	0.036 ± 0.035	0.106 ± 0.025
ALF	0.006 ± 0.012	0.002 ± 0.019	−0.005 ± 0.022[a]	0.018 ± 0.023	0.028 ± 0.020	0.000 ± 0.019

Note: All values represent micromolar (μM) OH*. Standard deviations are of measurements in triplicate. Graphical representation of this data can be found in Figure 4.

Abbreviation: R, reduced.

[a]Program to calculate hydroxyl radical concentrations will generate negative values for measurements below the detection limit.

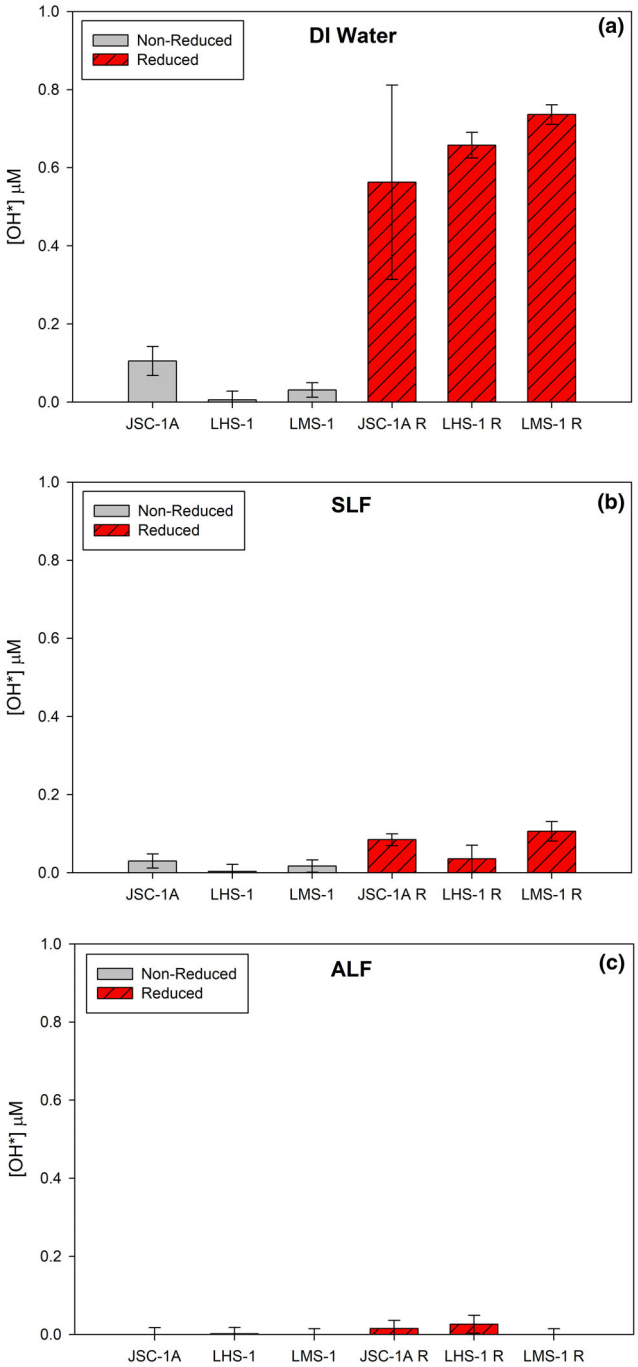

FIGURE 6. OH* generation from reduced and non-reduced JSC-1A, LHS-1, and LMS-1 in (a) DI water and the solutions, (b) SLF and (c) ALF. Used a particle loading of 100 m^2/L for all samples. Error bars represent standard deviations of measurements in triplicate. Numerical results can be found in Table 3. R, reduced.

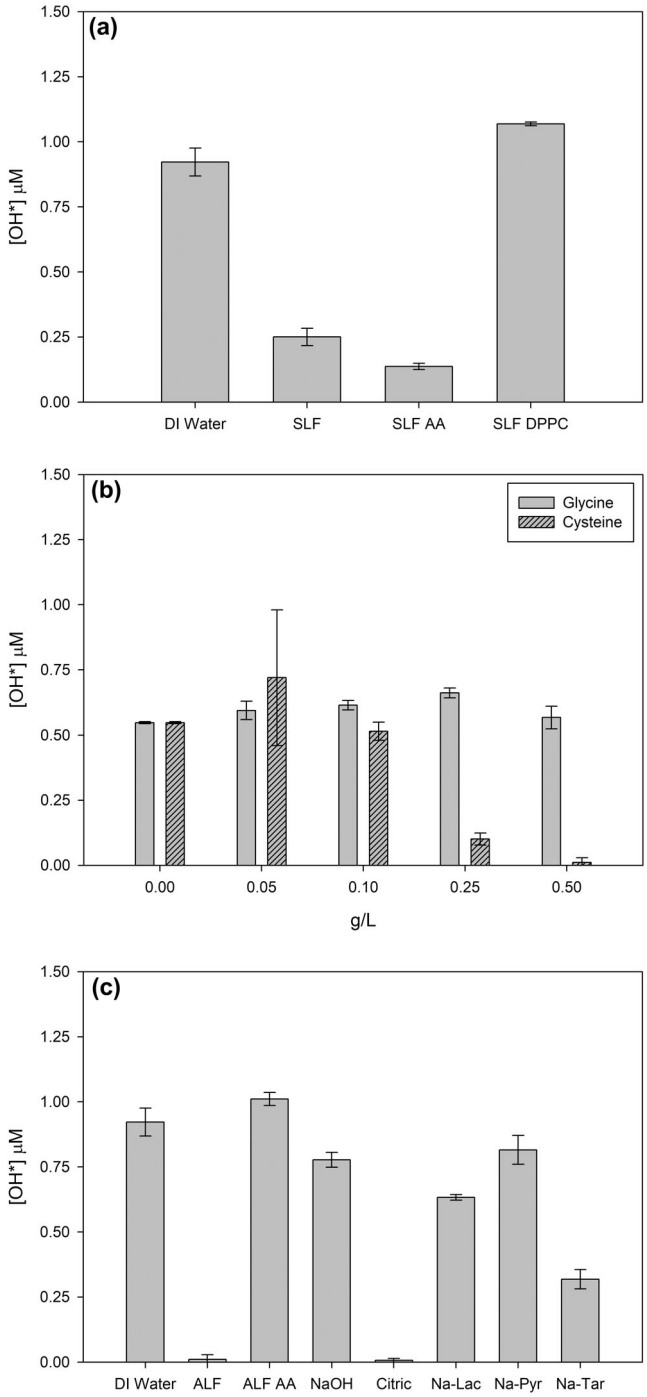

FIGURE 7. Generation of OH* in (a) DI water, SLF, and select components of SLF, and (b) individual concentrations of glycine and cysteine. (c) DI water, ALF, and select components of ALF. A particle loading of 400 m^2/L was used for all samples. AA, amino acid; ALF AA, 0.059 g/L glycine; Na-Lac, sodium lactate; Na-Pyr, sodium pyruvate; Na-Tar, sodium tartrate; SLF AA, 0.375 g/L glycine +0.121 g/L cysteine.

range used, and the reactivity is the same as for DI water. Cysteine on the other hand strongly mutes OH* formation at concentrations above 0.1 g/L. Notably, it appears that a large excess of cysteine is required to reduce the concentration of OH* produced.

Figure 7c shows the OH* generated by olivine in DI, ALF, and selected components of ALF, focusing largely on the organic components of this biological fluid simulant. As shown, glycine in isolation at the relevant concentration for ALF (0.06 g/L) is non-reactive toward OH*, consistent with the behavior described previously (Figure 7b). Tartrate, lactate, and pyruvate are also largely non-reactive toward OH*, as is the strong base, NaOH. The one component of ALF that appears to react toward OH* is citric acid, which nearly quantitatively removes OH* from solution at the high (20 g/L) concentration of citric acid in ALF.

DISCUSSION

We have demonstrated the ability to produce fresh "lunar-like" material and assess its generation of OH*. These simulant materials provide the opportunity to evaluate the processes by which oxidative radical species are generated, the potential impact of space weathering processes on reactivity, and the interactions that may take place between lunar dust and biological fluids upon inhalation exposure to lunar dust. The median particle sizes of our simulants range between 3 and 6 μm in diameter (Table 4) which is the size that is considered respirable and can be deposited in the alveolar regions of the lungs, therefore, these assays represent the oxidative potential of inhaled lunar particulate matter that would settle deep within the human respiratory system (Horwell, 2007; Jurinski & Rimstidt, 2001; Linnarsson et al., 2012). Both non-reduced JSC-1A and LMS-1 generate OH* in DI water, while LHS-1 generates much less in comparison (Figure 6a). This result is consistent with the hypothesis that iron is a necessary component in the generation of OH*, likely via surface-mediated Fenton chemistry, as observed in numerous prior studies. It is also clear from Figure 6a that our reduction technique leads to a sharp rise in OH* generation, and this is likely due to metallic iron, which we demonstrated is present using a variety of solid phase characterization techniques (Figures 1–4). The large increase in OH* generation, even for reduced LHS-1 in DI water, demonstrates the strong role that surficial metallic iron plays in the generation of OH* as compared to ferrous iron bound to oxygen in minerals and glass (the dominant valence state of iron in our non-reduced simulant materials). Our results are entirely consistent with those of Wallace et al. (2010), who showed a strong correlation between maturity and OH* generation. It is worth noting, however, that in lunar samples, metallic iron particles are often encapsulated in agglutinitic glass, and would require mechanical grinding to expose them at the surface for fluid interaction, as was done by Wallace et al. (2010). This exposure may be accomplished on the surface of the Moon by micrometeorite impacts. In the case of our chemically reduced simulants, metallic iron is present at particle surfaces, and thus readily available for interaction when suspended in fluid. Possibly countering the potential lower availability of metallic iron in mature lunar regolith, is the smaller grains size. Metallic iron particles in lunar agglutinates range between 3 and 33 nm, and are significantly smaller than the metallic iron particles produced in our study (Morris, 1980; Taylor et al., 2005). A detailed analysis of how size and surface area of small metallic iron particles affect OH* generation is beyond the scope of this study, but it is reasonable to expect that smaller particles with larger surface area/volume ratio might be more reactive, and thus our reduced simulants might underestimate the reactivity of smaller nanophase metallic iron particles native to the lunar regolith. Future studies should compare the reactivity of reduced simulants to those outlined in Kohout et al. (2014), which uses a two-step reduction method that results in metallic iron particles ranging between 5 and 20 nm (Kohout et al., 2014).

Measurable OH* quantities in both SLF and ALF were greatly reduced. The exact mechanisms at play regarding these observations are unknown due to the complexity of both the fluids and potential interactions between the fluids and dust samples. Some OH* was above the detection limit for both reduced JSC-1A and LMS-1 in SLF, which is likely due to the increased ability of metallic iron to generate OH* in solution. SLF and ALF contain various chelating agents that may be able to bind to iron and other surficial defect sites rendering them inactive in their ability to generate OH*. Experiments using olivine indicated that citric acid may be responsible for the reduction of measurable OH* in solution due to the possibility of it binding to surficial iron. These results seem contradictory due to the fact that macrophages are known to generate reactive oxygen species (ROS), such as hydrogen peroxide when activated by foreign particulate matter, which can then result in large quantities of generated OH* (Schoonen et al., 2006).

There is another process that may come into play, which could lead to potentially deleterious health consequences for future astronauts. This involves the oxidation of amino acids in solution (Harris & Silberman, 1983; Hawkins & Davies, 2001; Nagy & Floyd, 1984; Stadtman, 1990; Stadtman & Berlett, 1991; Stadtman & Levine, 2003). It was first proposed that OH* generated in a Fenton system can be scavenged by amino

TABLE 4. Median grain size and surface area calculated for lunar simulants.

Sample	JSC-1A	LMS-1	LHS-1	JSC-1A (R)	LMS-1 (R)	LHS-1 (R)
Surface area (m^2/g)	2.979	8.755	5.038	1.626	2.957	2.747
Median grain size ± SD (μm)	5.771 ± 0.023	5.343 ± 0.369	4.342 ± 0.072	6.356 ± 0.435	4.253 ± 0.014	3.501 ± 0.011

Note: Standard deviations are for three runs. Raw data for all samples can be found in supplemental Tables S2–S5.
Abbreviation: R, reduced.

acids in solution (Nagy & Floyd, 1984). This study observed that cysteine, which is a component of SLF, decreased the amount of measurable OH* in solution. There was no decrease in measurable OH* in glycine, mirroring our observations. Using a rate constant of (k_{DMPO}) $2.0 \times 10^9\ M^{-1}\ s^{-1}$ for the reaction between DMPO and OH*, an OH* concentration of 0.55×10^{-6} M, a DMPO concentration of 44×10^{-3} M, and the second-order rate equation $R_{DMPO} = k_{DMPO}[OH^*][DMPO]$ yields a rate of 4.84 M/s (Marriott et al., 1980). Using a rate constant of (k_{cys}) $5.35 \times 10^9\ M^{-1}\ s^{-1}$ for the reaction between cysteine and OH*, a cysteine concentration of 4×10^{-3} M, an OH* concentration of 0.55×10^{-6} M, and the second-order rate equation $R_{cys} = k_{cys}[OH^*][cys]$ yields a rate of 11.77 M/s (Mezyk, 1996). Therefore, the rate of reaction of cysteine with OH* is over twice as fast as is with DMPO and OH*. The pH-dependent rate constant for the cysteine-OH* reaction was calculated using a modified version of eqn. 15 in Mezyk (1996), though we had to switch their k_7 and k_{12} values to reproduce their Figure 6, which shows the relationship between pH and rate constant of the cysteine-OH* reaction (Mezyk, 1996). If k is higher for reactions between OH* and specific amino acids, then the OH* will more readily react with other amino acids compared to the spin-trap DMPO. The hydrogen-transfer (HT) reaction between the thiol group (−SH) in free cysteine and the OH* radical has a rate constant of 1.9×10^{10} M/s, lower than the rate constant of the DMPO-OH* reaction, which seems to be the opposite of what we would expect based on the low measured OH* concentrations in cysteine, perhaps indicating that the rate constant for the HT reaction requires revision, or that we need to account for how the specific conditions of our experiment (pH, T, DMPO, and cysteine concentrations) impact the relative rates of reaction (Romero-Silva et al., 2018).

This is the first study to assess the potential environmental health risks for future lunar astronauts using experimentally reduced simulants in biologically relevant fluids. This work has found the following:

- Lunar regolith simulants that mimic mature, reduced lunar regolith can be synthesized and used for reactivity studies.
- Reduced lunar simulants exhibit an increased ability to generate OH*, likely due to metallic iron.
- We predict reduced lunar dust simulants would strongly react with amino acids and proteins, which means exposure of our simulants to any living organisms would lead to negative health outcomes.
- Low levels of OH* measured in biological fluids are likely due to its interaction with amino acids.
- If these results mirror those of in situ lunar dust, we expect inhaled lunar dust to react with and denature proteins, which would be harmful to any living beings exposed to said dust.

It is noteworthy to discuss the results of the recently published manuscript by Chang et al. (2024), which shows that reduced lunar dust simulants used in this study contributed to observed elevated levels of toxicity to human lung alveolar epithelial (A549) cells, mitochondrial DNA, and nuclear DNA relative to the same non-reduced lunar dust simulants (Chang et al., 2024). The addition of N-acetylcysteine (NAC) to cells observed an across-the-board reduction in cytotoxic effects from all lunar dust simulant samples, indicating that free radicals (i.e., OH*) play a role in the observed increased cytotoxicity of reduced lunar dust simulants (Chang et al., 2024). This seems to indicate that the observed increase in OH* in this work translates to increased cytotoxicity observed by Chang et al. (2024). Other studies, such as (Caston et al., 2018; Lam et al., 2022), have shown no observed correlation between cytotoxicity and OH* generation potential. We theorize that cytotoxicity and OH* generation are potentially correlated but in an unknown way that requires much further study. The authors would like to add that OH* generation is one of many components of dust toxicity and more studies need to confirm the relative impact of free radicals on living cells versus other contributing factors (i.e., grain size, particle shape, and bioaccessibility). Damage from free radicals may play a larger role in observed cytotoxicity for particles with metallic iron versus without.

Assessment of OH* generation in each individual component of SLF and ALF is the next logical step in understanding the mechanisms of OH* generation in biological media. Toxicity/animal assays using reduced lunar simulants would enable comparison with previous studies that used Apollo 14 samples in mice assays (Lam et al., 2013; Scully & Meyers, 2015). High-performance liquid chromatography (HPLC) measurements such as

the ones conducted by Liu et al. (2017) for lunar dust simulants incubated in amino acids would be the next logical step in solving the discrepancy between the observed reduced OH* measured in cysteine and the higher k value for the reaction of DMPO and OH* (Liu et al., 2017).

Acknowledgments—The authors thank Jim Quinn who obtained SEM/EDS measurements for our lunar simulant samples. The authors also thank Allison Zastrow for obtaining reflectance measurements of lunar simulants and processing spectral data. The authors thank Jordan Young for writing the program to calculate OH* concentrations of sample incubations which can be found at https://github.com/dhendrix10/Donald-Work. Finally, the authors gratefully acknowledge Carle Pieters and A.J. Timothy Jull for editorial handling and an anonymous reviewer for helpful comments that improved the quality of the manuscript.

Funding Information—This work was supported by the RISE2 node of the NASA Solar System Exploration Research Virtual Institute (SSERVI) under agreement NNA114AB04A.

Conflict of Interest Statement—The authors declare that they have nothing to disclose.

Data Availability Statement—Data are available from the authors upon request.

Editorial Handling—Dr. A. J. Timothy Jull

REFERENCES

Allen, C. 2005. Biological Effects of Lunar Dust Workshop.

Allen, C. C., Morris, R. V., and McKay, D. S. 1994. Experimental Reduction of Lunar Mare Soil and Volcanic Glass. *Journal of Geophysical Research: Planets* 99(E11): 23173–85.

Angelé-Martínez, C., Goodman, C., and Brumaghim, J. 2014. Metal-Mediated DNA Damage and Cell Death: Mechanisms, Detection Methods, and Cellular Consequences. *Metallomics* 6: 1358–81.

Bos, P. M., Gosens, I., Geraets, L., Delmaar, C., and Cassee, F. R. 2019. Pulmonary Toxicity in Rats Following Inhalation Exposure to Poorly Soluble Particles: The Issue of Impaired Clearance and the Relevance for Human Health Hazard and Risk Assessment. *Regulatory Toxicology and Pharmacology* 109: 104498.

Brady, T. K., Winterhalter, D., Levine, J. S., and Kerschmann, R. L. 2020. Lunar Dust and Its Impact on Human Exploration: A NASA Engineering and Safety Center (NESC) Workshop.

Brain, J. D. 1992. Mechanisms, Measurement, and Significance of Lung Macrophage Function. *Environmental Health Perspectives* 97: 5–10.

Caston, R., Luc, K., Hendrix, D., Hurowitz, J. A., and Demple, B. 2018. Assessing Toxicity and Nuclear and Mitochondrial DNA Damage Caused by Exposure of Mammalian Cells to Lunar Regolith Simulants. *Geohealth* 2: 139–148.

Chang, J., Xue, Z., Bauer, J., Wehle, B., Hendrix, D., Catalano, T., Hurowitz, J., Nekvasil, H., and Demple, B. 2024. Artificial Space Weathering to Mimic Solar Wind Enhances the Toxicity of Lunar Dust Simulants in Human Lung Cells. *GeoHealth* 8: e2023GH000840.

Colombo, C., Monhemius, A. J., and Plant, J. A. 2008. Platinum, Palladium and Rhodium Release from Vehicle Exhaust Catalysts and Road Dust Exposed to Simulated Lung Fluids. *Ecotoxicology and Environmental Safety* 71: 722–730.

Dizdaroglu, M., Rao, G., Halliwell, B., and Gajewski, E. 1991. Damage to the DNA Bases in Mammalian Chromatin by Hydrogen Peroxide in the Presence of Ferric and Cupric Ions. *Archives of Biochemistry and Biophysics* 285: 317–324.

Eaton, G. R., Eaton, S. S., Barr, D. P., and Weber, R. T. 2010. *Quantitative EPR*. Berlin, Germany: Springer Science & Business Media.

Ehrlich, R., Akugizibwe, P., Siegfried, N., and Rees, D. 2021. The Association between Silica Exposure, Silicosis and Tuberculosis: A Systematic Review and Meta-Analysis. *BMC Public Health* 21: 953.

Fenton, H. 1894. LXXIII.—Oxidation of Tartaric Acid in Presence of Iron. *Journal of the Chemical Society, Transactions* 65: 899–910.

Fubini, B., and Fenoglio, I. 2007. Toxic Potential of Mineral Dusts. *Elements* 3: 407–414.

Fubini, B., Fenoglio, I., Elias, Z., and Poirot, O. 2001. Variability of Biological Responses to Silicas: Effect of Origin, Crystallinity, and State of Surface on Generation of Reactive Oxygen Species and Morphological Transformation of Mammalian Cells. *Journal of Environmental Pathology, Toxicology and Oncology* 20 (Suppl. 1): 95–108.

Fubini, B., and Hubbard, A. 2003. Reactive Oxygen Species (ROS) and Reactive Nitrogen Species (RNS) Generation by Silica in Inflammation and Fibrosis. *Free Radical Biology and Medicine* 34: 1507–16.

Gaier, J. R. 2008. The Need for High Fidelity Lunar Regolith Simulants.

Glenn, R. E., Craft, B. F., and Merchant, J. 1986. Air Sampling for Particulates. *DHHS (NEDSH) Pub (86–102)*: 69–82.

Hapke, B. 2001. Space Weathering from Mercury to the Asteroid Belt. *Journal of Geophysical Research: Planets* 106: 10039–73.

Hapke, B., Cohen, A., Cassidy, W., and Wells, E. 1970. Solar Radiation Effects in Lunar Samples. *Science* 167: 745–47.

Hardy, J. A., and Aust, A. E. 1995. Iron in Asbestos Chemistry and Carcinogenicity. *Chemical Reviews* 95: 97–118.

Harris, W. R., and Silberman, D. 1983. Time-Dependent Leaching of Coal Fly Ash by Chelating Agents. *Environmental Science & Technology* 17: 139–145.

Hawkins, C. L., and Davies, M. J. 2001. Generation and Propagation of Radical Reactions on Proteins. *Biochimica et Biophysica Acta (BBA)-Bioenergetics* 1504: 196–219.

He, M., Ichinose, T., Yoshida, S., Ito, T., He, C., Yoshida, Y., Arashidani, K., Takano, H., Sun, G., and Shibamoto, T. 2017. PM2. 5-Induced Lung Inflammation in Mice:

Differences of Inflammatory Response in Macrophages and Type II Alveolar Cells. *Journal of Applied Toxicology* 37: 1203–18.

Heiken, G. H., Vaniman, D. T., and French, B. M. 1991. *Lunar Sourcebook—A User's Guide to the Moon. Research Supported by NASA*. Cambridge, England: Cambridge University Press. 753.

Hendrix, D. A., Hurowitz, J. A., Glotch, T. D., and Schoonen, M. A. 2021. Olivine Dissolution in Simulated Lung and Gastric Fluid as an Analog to the Behavior of Lunar Particulate Matter inside the Human Respiratory and Gastrointestinal Systems. *GeoHealth* 5: e2021GH000491.

Hendrix, D. A., Port, S. T., Hurowitz, J. A., and Schoonen, M. A. 2019. Measurement of OH* Generation by Pulverized Minerals Using Electron Spin Resonance Spectroscopy and Implications for the Reactivity of Planetary Regolith. *Geohealth* 3: 28–42.

Hickson, C. J., and Juras, S. J. 1986. Sample Contamination by Grinding. *The Canadian Mineralogist* 24: 585–89.

Hill, E., Mellin, M. J., Deane, B., Liu, Y., and Taylor, L. A. 2007. Apollo Sample 70051 and High-and Low-Ti Lunar Soil Simulants MLS-1A and JSC-1A: Implications for Future Lunar Exploration. *Journal of Geophysical Research: Planets* 112.

Horwell, C. J. 2007. Grain-Size Analysis of Volcanic Ash for the Rapid Assessment of Respiratory Health Hazard. *Journal of Environmental Monitoring* 9: 1107–15.

Hörz, F., Hartung, J., and Gault, D. 1971. Micrometeorite Craters on Lunar Rock Surfaces. *Journal of Geophysical Research* 76: 5770–98.

Housley, R. M., Grant, R. W., and Paton, N. 1973. Origin and Characteristics of Excess Fe Metal in Lunar Glass Welded Aggregates. *Lunar and Planetary Science Conference Proceedings*, pp. 2737. Abstract #1119.

Hurowitz, J. A., Tosca, N. J., McLennan, S. M., and Schoonen, M. A. 2007. Production of Hydrogen Peroxide in Martian and Lunar Soils. *Earth and Planetary Science Letters* 255: 41–52.

James, J. T., Lam, C., Scully, R. R., Meyers, V. E., and McCoy, J. 2014. *Lunar Dust Toxicity: Final Report*. NASA. 16.

Jurinski, J. B., and Rimstidt, J. D. 2001. Biodurability of Talc. *American Mineralogist* 86: 392–99.

Kastury, F., Smith, E., Karna, R. R., Scheckel, K. G., and Juhasz, A. 2018. Methodological Factors Influencing Inhalation Bioaccessibility of Metal (Loid) s in PM2. 5 Using Simulated Lung Fluid. *Environmental Pollution* 241: 930–37.

Kaur, J., Rickman, D., and Schoonen, M. A. 2016. Reactive Oxygen Species (ROS) Generation by Lunar Simulants. *Acta Astronautica* 122: 196–208.

Keller, L. P., and McKay, D. S. 1997. The Nature and Origin of Rims on Lunar Soil Grains. *Geochimica et Cosmochimica Acta* 61: 2331–41.

Kohout, T., Čuda, J., Filip, J., Britt, D., Bradley, T., Tuček, J., Skála, R., Kletetschka, G., Kašlík, J., and Malina, O. 2014. Space Weathering Simulations Through Controlled Growth of Iron Nanoparticles on Olivine. *Icarus* 237: 75–83.

Lam, C.-W., Castranova, V., Zeidler-Erdely, P. C., Renne, R., Hunter, R., McCluskey, R., Scully, R. R., Wallace, W. T., Zhang, Y., and Ryder, V. E. 2022. Comparative Pulmonary Toxicities of Lunar Dusts and Terrestrial Dusts (TiO_2 & SiO_2) in Rats and an Assessment of the Impact of Particle-Generated Oxidants on the Dusts' Toxicities. *Inhalation Toxicology* 34: 51–67.

Lam, C.-W., Scully, R. R., Zhang, Y., Renne, R. A., Hunter, R. L., McCluskey, R. A., Chen, B. T., et al. 2013. Toxicity of Lunar Dust Assessed in Inhalation-Exposed Rats. *Inhalation Toxicology* 25: 661–678.

Li, M., Thompson, K. K., Nissen, J. C., Hendrix, D., Hurowitz, J. A., and Tsirka, S. E. 2019. Lunar Soil Simulants Alter Macrophage Survival and Function. *Journal of Applied Toxicology* 39: 1413–23.

Linnarsson, D., Carpenter, J., Fubini, B., Gerde, P., Karlsson, L. L., Loftus, D. J., Prisk, G. K., Staufer, U., Tranfield, E. M., and van Westrenen, W. 2012. Toxicity of Lunar Dust. *Planetary and Space Science* 74: 57–71.

Liu, F., Lai, S., Tong, H., Lakey, P. S. J., Shiraiwa, M., Weller, M. G., Pöschl, U., and Kampf, C. J. 2017. Release of Free Amino Acids upon Oxidation of Peptides and Proteins by Hydroxyl Radicals. *Analytical and Bioanalytical Chemistry* 409: 2411–20.

Liu, Y., and Taylor, L. A. 2011. Characterization of Lunar Dust and a Synopsis of Available Lunar Simulants. *Planetary and Space Science* 59: 1769–83.

Liu, Y., Taylor, L. A., Thompson, J. R., Schnare, D. W., and Park, J.-S. 2007. Unique Properties of Lunar Impact Glass: Nanophase Metallic Fe Synthesis. *American Mineralogist* 92: 1420–27.

Loftus, D., Rask, J., McCrossin, C., and Tranfield, E. 2010. The Chemical Reactivity of Lunar Dust: From Toxicity to Astrobiology. *Earth, Moon, and Planets* 107: 95–105.

Marriott, P. R., Perkins, M. J., and Griller, D. 1980. Spin Trapping for Hydroxyl in Water: A Kinetic Evaluation of Two Popular Traps. *Canadian Journal of Chemistry* 58: 803–7.

McKay, D. S., Carter, J. L., Boles, W. W., Allen, C. C., and Allton, J. H. 1994. JSC-1: A New Lunar Soil Simulant. *Engineering, Construction, and Operations in Space IV* 2: 857–866.

Merchant, J. A., Boehlecke, B. A., and Taylor, G. 1986. *Occupational Respiratory Diseases*. Washington, DC: US Department of Health and Human Services, Public Health Service.

Meza-Figueroa, D., Barboza-Flores, M., Romero, F. M., Acosta-Elias, M., Hernández-Mendiola, E., Maldonado-Escalante, F., Pérez-Segura, E., González-Grijalva, B., Meza-Montenegro, M., and García-Rico, L. 2020. Metal Bioaccessibility, Particle Size Distribution and Polydispersity of Playground Dust in Synthetic Lysosomal Fluids. *Science of the Total Environment* 713: 136481.

Mezyk, S. P. 1996. Determination of the Rate Constant for the Reaction of Hydroxyl and Oxide Radicals with Cysteine in Aqueous Solution. *Radiation Research* 145: 102–6.

Midander, K., Wallinder, I. O., and Leygraf, C. 2007. In Vitro Studies of Copper Release from Powder Particles in Synthetic Biological Media. *Environmental Pollution* 145: 51–59.

Morris, R. 1980. Origins and Size Distribution of Metallic Iron Particles in the Lunar Regolith. *Lunar and Planetary Science Conference Proceedings*, pp. 1697–1712. Abstract #1267.

Morton, N. 1989. Pulmonary Surfactant: Physiology, Pharmacology and Clinical Uses. *British Journal of Hospital Medicine* 42: 52–58.

Munn, N. J., Thomas, S. W., and DeMesquita, S. 1990. Pulmonary Function in Commercial Glass Blowers. *Chest* 98: 871–74.

Nagy, I. Z., and Floyd, R. A. 1984. Hydroxyl Free Radical Reactions with Amino Acids and Proteins Studied by Electron Spin Resonance Spectroscopy and Spin-Trapping. *Biochimica et Biophysica Acta (BBA)—Protein Structure and Molecular Enzymology* 790: 238–250.

Pelfrêne, A., Cave, M. R., Wragg, J., and Douay, F. 2017. In Vitro Investigations of Human Bioaccessibility from Reference Materials Using Simulated Lung Fluids. *International Journal of Environmental Research and Public Health* 14: 112.

Pieters, C. M., Taylor, L. A., Noble, S. K., Keller, L. P., Hapke, B., Morris, R. V., Allen, C. C., McKay, D. S., and Wentworth, S. 2000. Space Weathering on Airless Bodies: Resolving a Mystery with Lunar Samples. *Meteoritics & Planetary Science* 35: 1101–7.

Portree, D. S. 1997. *Walking to Olympus: An EVA Chronology*. NASA Headquarters: NASA History Office, Office of Policy and Plans.

Pryor, W. 1988. Why is the OH* the Only Radical that Commonly Adds to DNA—Hypothesis—It has a Rare Combination of High Electrophilicity, High Thermochemical Reactivity, and a Mode of Production that can Occur near DNA. *Free Radical Biology and Medicine* 4: 219–223.

Romero-Silva, A., Mora-Diez, N., and Alvarez-Idaboy, J. R. 2018. Theoretical Study of the Reactivity and Selectivity of Various Free Radicals with Cysteine Residues. *ACS Omega* 3: 16519–28.

Sankila, R., Karjalainen, S., Pukkala, E., Oksanen, H., Hakulinen, T., Teppo, L., and Hakama, M. 1990. Cancer Risk among Glass Factory Workers: An Excess of Lung Cancer? *Occupational and Environmental Medicine* 47: 815–18.

Scheuring, R. A., Jones, J. A., Novak, J. D., Polk, J. D., Gillis, D. B., Schmid, J., Duncan, J. M., and Davis, J. R. 2008. The Apollo Medical Operations Project: Recommendations to Improve Crew Health and Performance for Future Exploration Missions and Lunar Surface Operations. *Acta Astronautica* 63: 980–87.

Schoonen, M. A., Cohn, C. A., Roemer, E., Laffers, R., Simon, S. R., and O'Riordan, T. 2006. Mineral-Induced Formation of Reactive Oxygen Species. *Reviews in Mineralogy and Geochemistry* 64: 179–221.

Scully, R. R., and Meyers, V. E. 2015. Risk of Adverse Health and Performance Effects of Celestial Dust Exposure.

Shearer, C., Eppler, D., Farrell, W., Gruener, J., Lawrence, S., Pellis, N., Spudis, P., Stopar, J., Zeigler, R., and Neal, C. 2016. Results of the lunar exploration analysis group (LEAG) gap review: Specific action team (SAT), examination of strategic knowledge gaps (SKGs) for human exploration of the moon. In 2016 Annual Meeting of the Lunar Exploration Analysis Group (20160012743).

Stadtman, E., and Levine, R. 2003. Free Radical-Mediated Oxidation of Free Amino Acids and Amino Acid Residues in Proteins. *Amino Acids* 25: 207–218.

Stadtman, E. R. 1990. Metal Ion-Catalyzed Oxidation of Proteins: Biochemical Mechanism and Biological Consequences. *Free Radical Biology and Medicine* 9: 315–325.

Stadtman, E. R., and Berlett, B. S. 1991. Fenton Chemistry. Amino Acid Oxidation. *Journal of Biological Chemistry* 266: 17201–11.

Stopford, W., Turner, J., Cappellini, D., and Brock, T. 2003. Bioaccessibility Testing of Cobalt Compounds. *Journal of Environmental Monitoring* 5: 675–680.

Taylor, L. 2008. *NASA's Dirty Secret: Moon Dust*. Palmyra, VA: News Wise.

Taylor, L., Schmitt, H., Carrier, W., and Nakagawa, M. 2005. The Lunar Dust Problem: From Liability to Asset. *1st Space Exploration Conference: Continuing the Voyage of Discovery. Conf., American Institute of Aeronautics and Astronautics.*

Taylor, L. A., and Meek, T. T. 2005. Microwave Sintering of Lunar Soil: Properties, Theory, and Practice. *Journal of Aerospace Engineering* 18: 188–196.

Taylor, L. A., Pieters, C. M., and Britt, D. 2016. Evaluations of Lunar Regolith Simulants. *Planetary and Space Science* 126: 1–7.

Thompson, M. S., Zega, T. J., Becerra, P., Keane, J. T., and Byrne, S. 2016. The Oxidation State of Nanophase Fe Particles in Lunar Soil: Implications for Space Weathering. *Meteoritics & Planetary Science* 51: 1082–95.

Turci, F., Corazzari, I., Alberto, G., Martra, G., and Fubini, B. 2015. Free-Radical Chemistry as a Means to Evaluate Lunar Dust Health Hazard in View of Future Missions to the Moon. *Astrobiology* 15: 371–380.

Von Sonntag, C. 1991. *Physical and Chemical Mechanisms in Molecular Radiation Biology*. New York: Plenum Press.

Wallace, W. T., Phillips, C. J., Jeevarajan, A. S., Chen, B., and Taylor, L. A. 2010. Nanophase Iron-Enhanced Chemical Reactivity of Ground Lunar Soil. *Earth and Planetary Science Letters* 295: 571–77.

Wallace, W. T., Taylor, L. A., Liu, Y., Cooper, B. L., McKay, D. S., Chen, B., and Jeevarajan, A. S. 2009. Lunar Dust and Lunar Simulant Activation and Monitoring. *Meteoritics & Planetary Science* 44: 961–970.

Wani, K., and Niyogi, A. 1968. Environment and Silicosis in Glass Factories. *Indian Journal of Public Health* 12: 131–39.

Weggeberg, H., Benden, T. F., Steinnes, E., and Flaten, T. P. 2019. Element Analysis and Bioaccessibility Assessment of Ultrafine Airborne Particulate Matter (PM0. 1) Using Simulated Lung Fluid Extraction (Artificial Lysosomal Fluid and Gamble's Solution). *Environmental Chemistry and Ecotoxicology* 1: 26–35.

Wiseman, C. L. 2015. Analytical Methods for Assessing Metal Bioaccessibility in Airborne Particulate Matter: A Scoping Review. *Analytica Chimica Acta* 877: 9–18.

Xu, C., Zhang, M., Chen, W., Jiang, L., Chen, C., and Qin, J. 2020. Assessment of Air Pollutant PM2. 5 Pulmonary Exposure Using a 3D Lung-on-Chip Model. *ACS Biomaterials Science & Engineering* 6: 3081–90.

SUPPORTING INFORMATION

Additional supporting information may be found in the online version of this article.

Figure S1. Normalized OH* generation data for various minerals. Particle loadings of 400 g L^{-1} used for all experiments. JSC-1A is not reduced/heat treated. Reproduced from Hendrix et al. (2019).

Figure S2. Particle size distribution graphs of (a) non-reduced lunar simulants and (b) reduced lunar simulants. Intensity refers to the intensity of the light scattered by the particles. Table S4 denotes the numerical values of all particle sizes.

Table S1. Vendor and catalog number of each component used in SLF and ALF.

Table S2. Parameters used for EPR measurements.

Table S3. Vendor and catalog number of all chemicals and standards used in this work NOT including those used in SLF and ALF (see Table S1).

Table S4. Particle size distribution of lunar simulant grains used in this study. Graphical data represented in Figure S3. Averages and standard deviations are of three runs. SD, standard deviation.

Table S5. Masses and surface areas of the aluminum oxide reference material (Anton Paar) for six separate standards run between March 2021 and April 2021. Error is the percent deviation from the expected reference standard value (14.26 $m^2 g^{-1}$).

Table S6. Surface areas calculated for all lunar simulants samples. Our measurements are reproducible and have a low error based on the data in Table S4.